# Substrate integrated waveguide resonator sensor for X-band dielectric constant characterization

Cite as: J. Appl. Phys. 138, 074503 (2025); doi: 10.1063/5.0280603

Submitted: 13 May 2025 · Accepted: 28 July 2025 ·

Published Online: 18 August 2025







Omaima Talmoudi, <sup>1, a)</sup> 📵 Álvaro Gómez-Gómez,² 📵 Oscar Fernandez,² 📵 Jaouad Terhzaz,³ Abdelwahed Tribak, ¹ and Tomás Fernández-Ibáñez<sup>2</sup>

#### **AFFILIATIONS**

- <sup>1</sup>Institut National des Postes et Télécommunications (INPT), Rabat, Morocco
- <sup>2</sup>Departamento de Ingeniería de Comunicaciones, Universidad de Cantabria, Santander, Spain
- <sup>3</sup>Centre Régional des Métiers de l'Éducation et de la Formation (CRMEF), Casablanca, Morocco

#### **ABSTRACT**

This work presents the design, simulation, and experimental validation of a compact single-port microwave sensor based on substrate integrated waveguide technology. The proposed sensor consists of a circular resonant cavity implemented in a substrate integrated waveguide, with a rosette-shaped slot etched into the top copper layer to enhance electric field confinement in the sensing region. This configuration enables the accurate characterization of low-permittivity materials in the X-band frequency range. The reflection response S11 of uration enables the accurate characterization of low-permittivity materials in the X-band frequency range. The reflection response  $S_{11}$  of  $\frac{1}{2}$  the sensor is analyzed for various materials, including air, Teflon, and Plexiglas. The results show a clear resonance frequency shift  $\frac{1}{2}$ depending on the permittivity of the material, with measured sensitivities of about 5.85% for Teflon and 3.65% for Plexiglas. The proposed structure shows good agreement between the simulation and the measurement results, as well as non-destructive characterization of dielectric properties, as the material under test is not physically or chemically altered during the measurement process.

© 2025 Author(s). All article content, except where otherwise noted, is licensed under a Creative Commons Attribution (CC BY) license (https://creativecommons.org/licenses/by/4.0/). https://doi.org/10.1063/5.0280603

#### I. INTRODUCTION

Microwave sensors have become an important technology for accurately characterizing dielectric materials due to their nondestructive nature, compact design, and real-time measurement capabilities.1 These sensors are used in various fields, such as food safety, biomedical diagnostics, materials science, and industrial processing.<sup>2-4</sup> Among the various techniques available for permittivity estimation, resonance methods have been widely adopted due to their superior sensitivity and accuracy compared to broadband alternatives.<sup>5,6</sup> Substrate Integrated Waveguide (SIW) technology has emerged as a powerful solution that integrates waveguide performance into a planar structure. SIW sensors offer significant advantages, such as low loss, high quality factors, ease of integration, and compatibility with printed circuit technology, making them particularly suitable for dielectric characterization in the GHz range.8 Operating in the 300 MHz to 300 GHz frequency range, microwave sensors based on SIW technology may offer unique capabilities, such as all-weather functionality and the ability to operate through various materials.9

Recent research has focused on optimizing sensor topologies and excitation mechanisms to enhance sensitivity, resolution, and miniaturization. Microwave sensors incorporating resonators, such as split-ring resonators (SRRs), complementary SRRs (CSRRs), and other metamaterial-inspired structures, have demonstrated improved electric field confinement, enabling high sensitivity to variations in the dielectric properties of the material under test. 4,5,10 The techniques involving CSRR configurations have shown significant improvements in field confinement and sensing capabilities for both solid and liquid materials. Furthermore, machine learning approaches, such as Artificial Neural Networks (ANNs), have been introduced to reconstruct permittivity from resonant parameters, enhancing accuracy and expanding applicability.1

The objective of this work is to design and develop a compact microwave sensor based on SIW technology for the accurate characterization of dielectric materials. The proposed sensor consists of a circular SIW resonant cavity, with a rosette-shaped slot etched into the top metal layer to enhance sensitivity and improve field interaction with the material under test.11

<sup>&</sup>lt;sup>a)</sup>Author to whom correspondence should be addressed: omaimatalmoudi@gmail.com

In addition, the long-term goal of this research is to extend the capability of the sensor to the characterization of different types of materials, including powders and liquids. This would increase the range of applications in areas, such as chemical sensing, biomedical diagnostics, and industrial quality control. The integration of such microwave sensing systems with emerging technologies, including artificial intelligence and Internet of Things (IoT) platforms, offers promising avenues for real-time monitoring and intelligent sensing in complex environments.

# II. DESIGN AND SIMULATION OF THE PROPOSED **SENSOR**

The sensor is developed using SIW technology, carefully dimensioned to ensure high-performance S<sub>11</sub> parameter measurements. Its compact footprint is defined by the substrate dimensions  $A \times B$ , where  $A = 16.5 \,\mathrm{mm}$  and  $B = 23.65 \,\mathrm{mm}$ , as illustrated in Fig. 1. A microstrip feed line of length  $L_m = 4.8 \,\mathrm{mm}$  transitions into a tapered section of length  $L_t = 3.87 \,\mathrm{mm}$  to facilitate smooth impedance matching. This transition enables mode conversion from the quasi-TEM mode of the microstrip line to the transverse electric (TE) mode supported by the SIW structure, minimizing reflection losses and enhancing the energy transfer into the cavity.

The tapered section leads to a circular SIW resonant cavity with a radius  $R = 8.25 \,\mathrm{mm}$ , placed within the substrate as shown in Fig. 1. At the center of this cavity lies a four-arm rosette-shaped slot, depicted in Fig. 2, patterned on the top metal layer. Each resonator arm has width  $W = 0.8 \,\mathrm{mm}$ , follows an arc of radius R=2 mm, and subtends an angular span of  $\alpha=180^{\circ}$ . The arc length L is related to the angular span by  $\alpha = \frac{L}{p}$ .

The circular geometry of the cavity is selected for its superior electromagnetic characteristics. Compared to the alternative cavity shapes, 14 it offers a more symmetric and uniform electric field distribution, reducing edge diffraction and enhancing field confinement near the center of the structure. This symmetry improves energy coupling to the resonator arms, leading to a higher quality factor (Q) and enhanced sensitivity to the variations in the dielectric properties.

The sensor is fabricated in a two-layer structure. The bottom layer comprises a full rectangular ground plane, while the top metal layer houses the rosette-shaped slot and feed line structures. The substrate used is Rogers RT/Duroid 4003, known for its low dielectric loss and stable electromagnetic performance at microwave

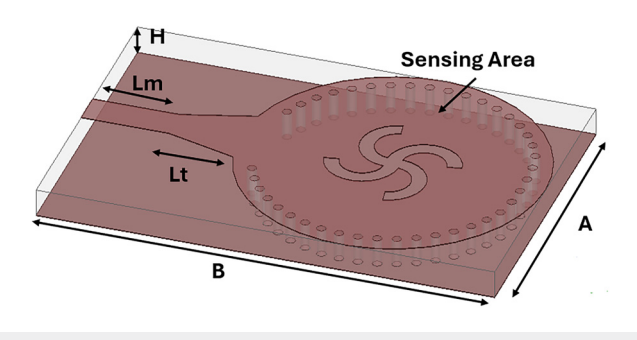


FIG. 1. 3D view of the full SIW sensor structure.

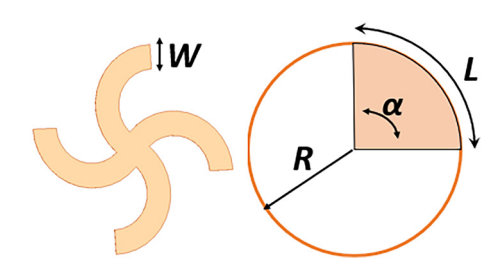


FIG. 2. Geometry of the rosette-shaped slot with four curved arms.

frequencies. The total height of the substrate is denoted by H = 1.52 mm, and the complete design is characterized by the transmission line lengths  $L_t$  and  $L_m$ , along with the overall footprint  $A \times B$ . Figures 1 and 2 illustrate the complete sensor layout and the detailed geometry of the resonator, respectively.

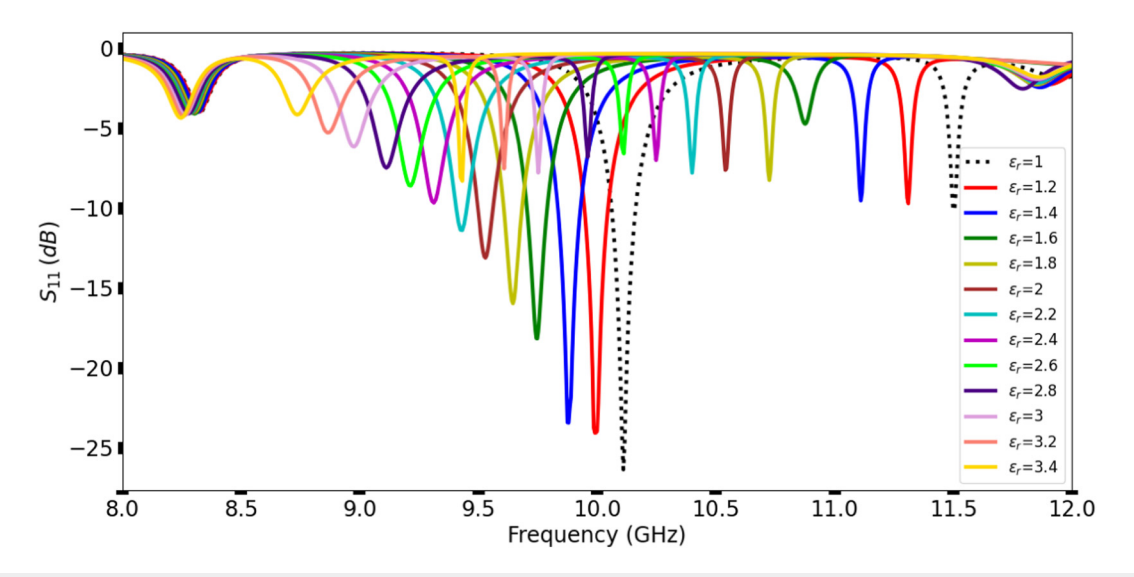
The sensor was modeled and analyzed using ANSYS HFSS to evaluate its performance in both empty and loaded configurations with different dielectric materials. The simulation environment was set up to study the behavior of the reflection coefficient  $(S_{11})$ , which is highly sensitive to the electromagnetic interaction between the sensor and the material under test.

To evaluate the sensitivity of the proposed SIW sensor to the variations in the dielectric properties, a parametric study was performed by varying the relative permittivity  $(\varepsilon_r)$  of the material under test (MUT). Sensitivity, in this context, recently of the sensor to detect small changes in permittivity by observing a life in the resonant frequency. The permittivity values were swept from 1.0 to 3.2 in 0.2 increments, allowing a detailed examination of how the resonant response of the sensor evolves with respect to the variations in  $\varepsilon_r$ . The obtained results are depicted in Fig. 3.

The simulated electric field distributions presented in Fig. 4 demonstrate the sensing behavior of the proposed structure at the resonance frequency and under an off-resonance condition. As shown in Fig. 4(a), the electric field is strongly confined around the rosette-shaped slot located at the center of the circular SIW cavity. This confinement significantly enhances the interaction between the resonant mode and the material under test. The sensor configuration maximizes the field intensity within the sensing region, enabling high sensitivity to dielectric perturbations.

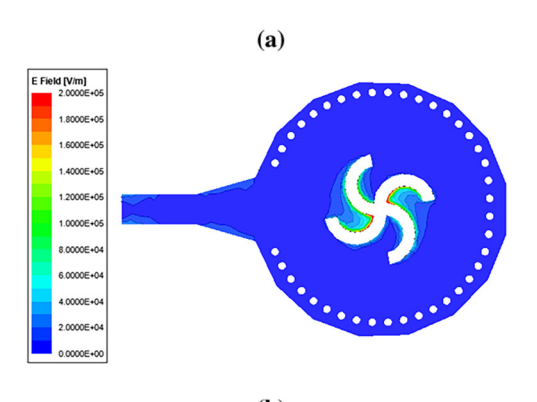
In contrast, Fig. 4(b) illustrates the field distribution at 9.75 GHz (off-resonance), where the field is notably weaker and less concentrated. This reduced confinement minimizes the interaction with the material under test, confirming the sensor's frequency-

Here, it is important to recall that the sensor configuration, which integrates a rosette-shaped slot into a circular SIW resonant cavity, provides good electric field confinement in the sensing region, enhancing the sensitivity to dielectric perturbations. As the dielectric constant  $(\varepsilon_r)$  of the MUT increases, the effective permittivity surrounding the resonator also increases, which causes the phase velocity of the guided wave to decrease and the resonant frequency to shift downward. These shifts are captured by the  $S_{11}$  parameter, with the resonance dips marking the frequencies of interest.



**FIG. 3.** Simulated  $S_{11}$  for MUT with varying  $\varepsilon_r$ .

The simulation results shown in Fig. 3, along with the values summarized in Table I, clearly confirm the sensor sensitivity to the variations in the dielectric constant. As  $\varepsilon_r$  increases from 1.0 to 3.4, the resonant frequency shifts down from 10.10 to 8.80 GHz,



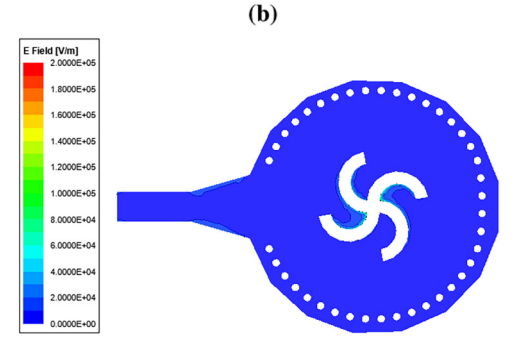


FIG. 4. Simulated electric field magnitude distribution of the proposed sensor: (a) at 10.10 GHz (on-resonance) and (b) at 9.75 GHz (off-resonance).

indicating a good correlation between material permittivity and the resonant response. At the same time, the notch depth becomes progressively shallower, reflecting a decrease in coupling efficiency and an increase in dielectric losses.

The plot in Fig. 5 shows the resonant frequency vs the dielectric constant of the MUT. The plot shows monotonic and nearly linear behavior over the frequency range studied, confirming the ability to use this relationship as a calibration basis for permittivity estimation. The observed sensitivity to small permittivity variations highlights the ability of the sensor to accurately discriminate between materials. tric constant of the MUT. The plot shows monotonic and nearly between materials.

These results validate the effectiveness of the proposed sensor, which is based on a circular SIW resonant cavity with a

TABLE I. Resonance behavior as a function of the dielectric constant of the material under test.

Dielectric constant $\varepsilon_r$ of MUT	Resonance frequency (GHz)	Notch depth (dB)
1.0	10.10	-26.35
1.2	9.90	-24.05
1.4	9.80	-23.43
1.6	9.70	-18.16
1.8	9.60	-15.96
2.0	9.50	-13.11
2.2	9.40	-11.37
2.4	9.30	-09.54
2.6	9.20	-08.60
2.8	9.10	-07.47
3.0	9.00	-06.15
3.2	8.90	-05.31
3.4	8.80	-04.22

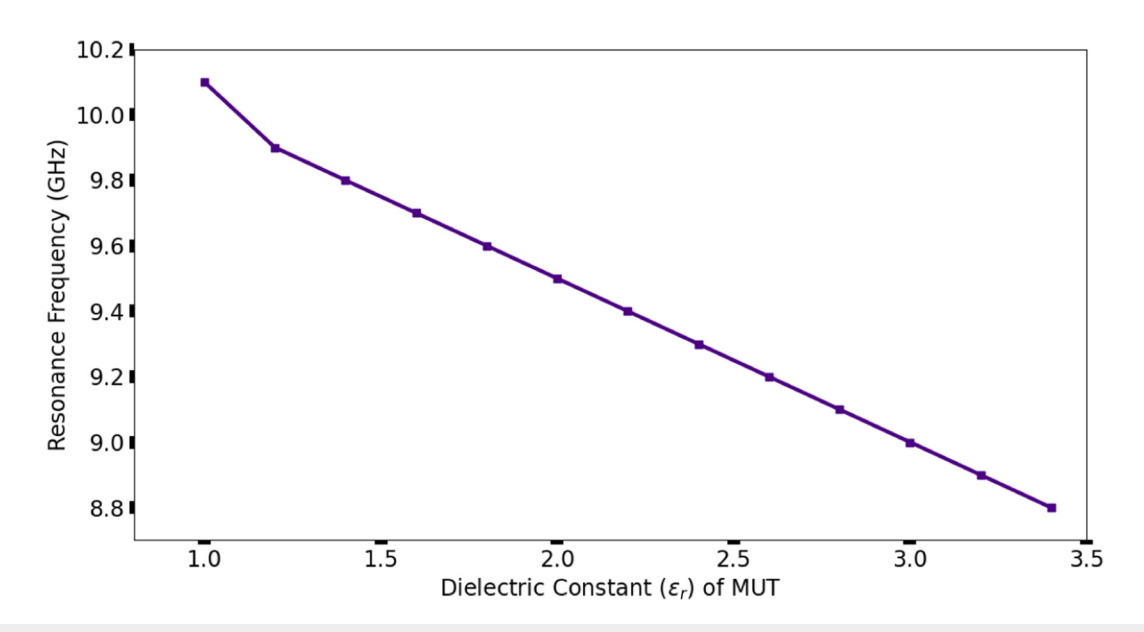
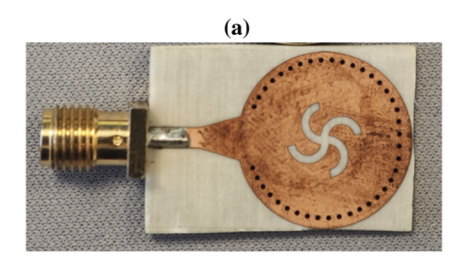


FIG. 5. Dielectric constant of MUT vs the resonance frequency of the sensor.



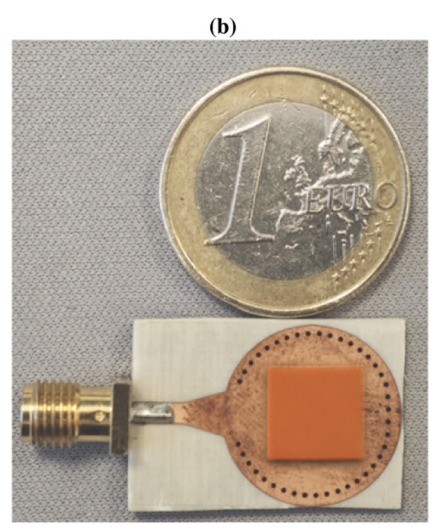


FIG. 6. Top view of (a) the fabricated SIW sensor with rosette and (b) the sensor with a sample of the material under test.

rosette-shaped slot, for accurate, real-time dielectric characterization in the X-band frequency range.

A calibration equation was derived from the simulation results to describe the observed linear behavior in Fig. 5 quantitatively. The relationship between the resonant frequency  $f_r$  (in GHz) and the The relationship between the resonant frequency  $f_r$  (in GHz) and the relative permittivity  $\varepsilon_r$  of the material under test was modeled using least squares linear regression, yielding the following expression:  $f_r = -0.516 \cdot \varepsilon_r + 10.544. \tag{1}$ 

$$f = 0.516 \cdot c + 10.544$$
 (1)

This analytical expression allows the dielectric constant of an unknown material to be estimated directly from its measured resonant frequency. By inverting the equation, the relative permittivity can be calculated as

$$\varepsilon_r = \frac{10.544 - f_r}{0.516}. (2)$$

# **III. EXPERIMENTAL MEASUREMENTS**

# A. Dielectric characterization and permittivity estimation

The proposed sensor was fabricated after the completion of the HFSS design and the optimization process, as shown in Fig. 6. To validate the electromagnetic model, a comparison between the simulated and measured reflection coefficients  $(S_{11})$  for the sensor was performed.

As shown in Fig. 7, which illustrates the variation of  $S_{11}$  vs frequency, the resonance frequency and the overall shape of the response curves exhibit good agreement between the simulation and the measurement.

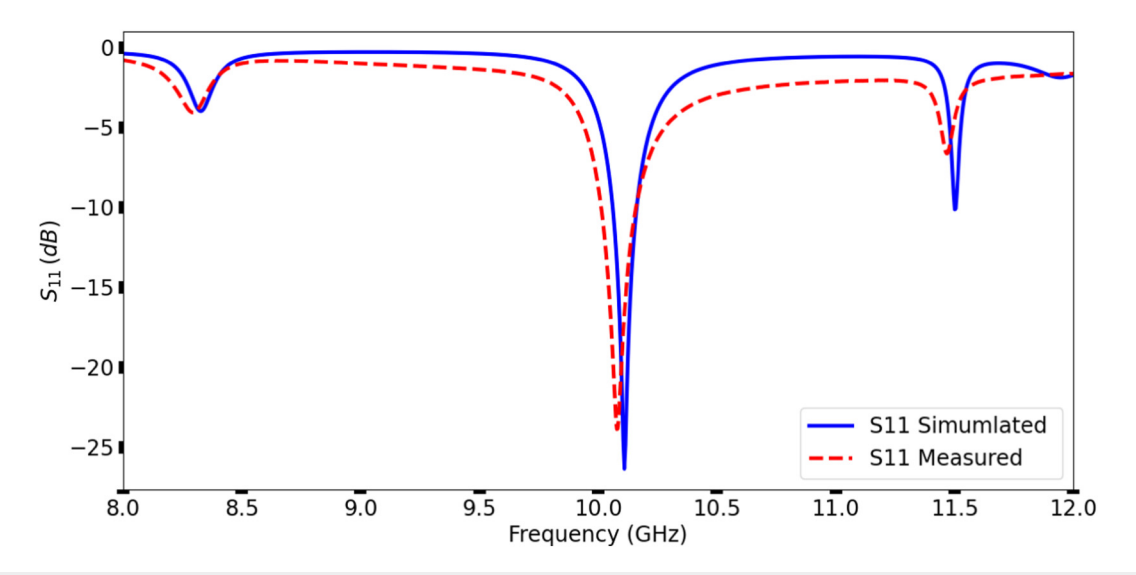


**FIG. 7.** Comparison of the simulated and measured  $S_{11}$  for the empty sensor.

To ensure the robustness of the proposed design, we analyzed the impact of minor fabrication tolerances and concluded that the differential frequency responses between the unloaded and loaded configurations are largely preserved. This confirms that the sensing mechanism is effective and reliable, despite the typical manufacturing variations.

The validated sensor was experimentally tested with three dielectric materials: air, Teflon, and Plexiglas, using a calibrated vector network analyzer (VNA). Each material was successively positioned over the sensing area of the fabricated device as presented in Figs. 1 and 6(b), and the reflection coefficient  $(S_{11})$  was measured over the X-band frequency range. The measured responses, shown in Fig. 8, exhibit significant resonance frequency shifts corresponding to each material, confirming the sensitivity of the sensor to the variations in the dielectric constant.

To evaluate and quantify the response of the proposed sensor to different dielectric materials, a parametric simulation study was previously conducted by varying the relative permittivity  $(\varepsilon_r)$  of the material under test. As reported in Table I, increasing the permittivity resulted in a systematic downward shift in the resonance

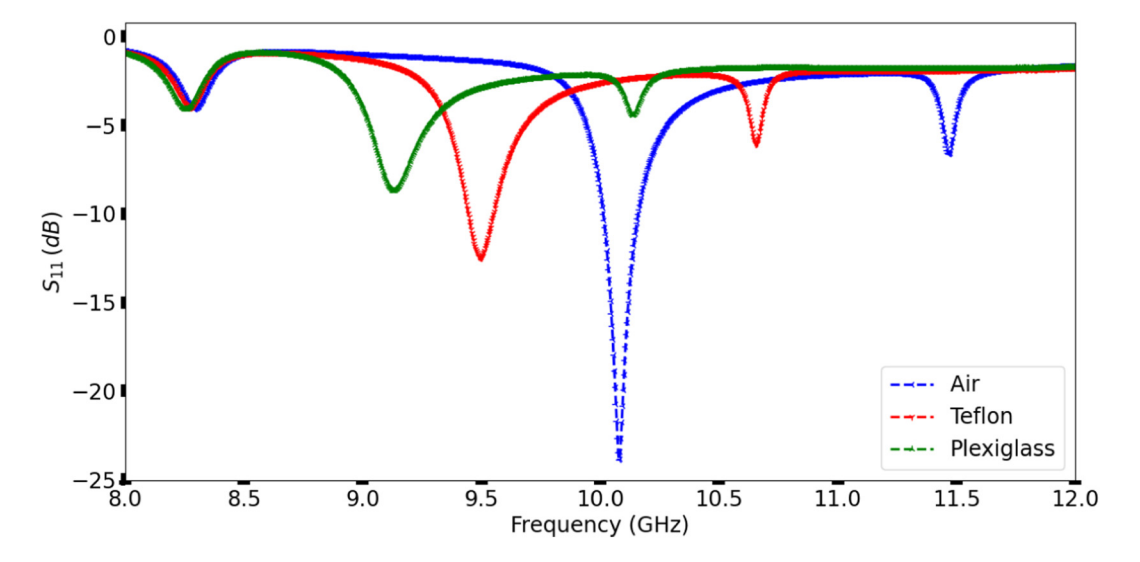


**FIG. 8.** Measured  $S_{11}$  for air, Teflon, and Plexiglas using the fabricated sensor.

TABLE II. Comparison of sensor sensitivity among various sensor types.

Reference	Sensor type	Operating frequency (GHz)	Sensitivity (%)
16	CSRR	2.65	3.98
17	SRR	2.41	3.63
18	IDC	3.316	5.05
19	Square SIW re-entrant	2.188 75	0.366
This work	Circular SIW with rosette	10.10	5.85

frequency, along with a gradual decrease in the notch depth. This trend can be attributed to the rise in effective permittivity within the sensing region, which modifies the phase velocity and alters the resonant behavior of the SIW cavity.

Using the linear model previously derived to describe the dependence of the resonant frequency on the material  $(\varepsilon_r)$ , the dielectric constants of air, Teflon, and Plexiglas were estimated from their measured responses, as shown in Fig. 5.

The observed frequencies 10.10 GHz for air, 9.50 GHz for Teflon, and 9.03 GHz for Plexiglas were inserted into the calibration equation to compute the corresponding permittivity values. The estimates obtained were approximately 1.00 for air, 2.02 for Teflon, and 2.94 for Plexiglas, which are in excellent agreement with the values reported in the literature. This close match validates both the accuracy of the simulation-based model and the practical effectiveness of the sensor design for dielectric characterization.

# B. Sensitivity and accuracy analysis

The sensitivity of the sensor was numerically evaluated by analyzing the relative shift in the resonant frequency when transitioning from air to each material under test using the mathematical expression proposed in Ref. 15,

$$S_{\varepsilon_r} = \frac{f_0 - f_r}{f_0(\varepsilon_r - 1)} \times 100,\tag{3}$$

where  $f_0$  is the resonance frequency with air,  $f_r$  is the resonance frequency with the material under test, and  $\varepsilon_r$  is the known relative permittivity.

The sensitivity for Teflon ( $\varepsilon_r \approx 2.02$ ) was calculated to be approximately 5.85%. For Plexiglas ( $\varepsilon_r \approx 2.94$ ), the sensitivity was found to be about 3.65%. These results demonstrate that the sensor maintains high sensitivity, particularly for low-permittivity materials.

A comparative overview with the other published microwave sensors is listed in Table II, confirming the competitiveness of the proposed design in sensitivity, where the bold value indicates the sensitivity obtained in this work.

# IV. SUMMARY AND CONCLUSIONS

The proposed microwave sensor, based on a circular SIW resonant cavity with a rosette-shaped slot etched into the top copper layer, enables the estimation of the dielectric constant of various materials within the X-band frequency range. The experimental results show good agreement with electromagnetic simulations, validating the proposed design. This agreement between the measured and simulated responses confirms the ability of the sensor to detect permittivity variations with good sensitivity. Its small size, compatible fabrication, and accurate operation in the X-band frequency range make it a promising candidate for practical applications in low-cost, high-resolution materials sensing.

# **ACKNOWLEDGMENTS**

This research was funded by the Spanish Ministry of Science and the European Union: MCIN/AEI/10.13039/501100011033/ FEDER, UE, Grant No. PID2022-137619NB-I00, and Project No. PGC2018-098350-B-C22. We are very grateful to Professor Jésus R. Pérez (Universidad de Cantabria) for his help with the measurements. We also thank Paul García Cadelo and Eva Mª Cuerno García, the technicians of the laboratory in Departamento de Ingeniería de Comunicaciones (Universidad de Cantabria), for their help in manufacturing the structures.

# **AUTHOR DECLARATIONS**

#### **Conflict of Interest**

The authors have no conflicts to disclose.

#### **Author Contributions**

Omaima Talmoudi: Conceptualization (equal); Data curation (equal); Formal analysis (equal); Funding acquisition (equal); & Investigation (equal); Methodology (equal); Project administration (equal); Resources (equal); Software (equal); Supervision (equal); Validation (equal); Visualization (equal); Writing – original draft (equal); Writing – review & editing (equal). **Álvaro Gómez-Gómez:** Conceptualization (equal); Data curation (equal); Formal analysis (equal); Funding acquisition (equal); Investigation (equal); 🖁 Methodology (equal); Project administration (equal); Resources (equal); Software (equal); Supervision (equal); Validation (equal); Visualization (equal); Writing - original draft (equal); Writing review & editing (equal). Oscar Fernandez: Conceptualization (equal); Data curation (equal); Formal analysis (equal); Funding acquisition (equal); Investigation (equal); Methodology (equal); Project administration (equal); Resources (equal); Software (equal); Supervision (equal); Validation (equal); Visualization (equal); Writing - original draft (equal); Writing - review & editing (equal). Jaouad Terhzaz: Conceptualization (equal); Data curation (equal); Formal analysis (equal); Funding acquisition (equal); Investigation (equal); Methodology (equal); Project administration (equal); Resources (equal); Software (equal); Supervision (equal); Validation (equal); Visualization (equal); Writing – original draft (equal); Writing – review & editing (equal). **Abdelwahed Tribak:** Conceptualization (equal); Data curation (equal); Formal analysis (equal); Funding acquisition (equal); Investigation (equal); Methodology (equal); Project administration (equal); Resources (equal); Software (equal); Supervision (equal); Validation (equal); Visualization (equal); Writing - original draft (equal); Writing editing review (equal). Tomás Fernández-Ibáñez: Conceptualization (equal); Data curation (equal); Formal analysis (equal); Funding acquisition (equal); Investigation (equal);

Methodology (equal); Project administration (equal); Resources (equal); Software (equal); Supervision (equal); Validation (equal); Visualization (equal); Writing – original draft (equal); Writing – review & editing (equal).

#### DATA AVAILABILITY

The data that support the findings of this study are available from the corresponding author upon reasonable request.

### **REFERENCES**

- <sup>1</sup>N. Javanbakht, G. Xiao, and R. E. Amaya, "A comprehensive review of portable microwave sensors for grains and mineral materials moisture content monitoring," IEEE Access 9, 120176–120184 (2021).
- <sup>2</sup>H.-L. Zhang, Q. Ma, L.-F. Fan, P.-F. Zhao, J.-X. Wang, X.-D. Zhang, D.-H. Zhu, L. Huang, D.-J. Zhao, and Z.-Y. Wang, "Nondestructive in situ measurement method for kernel moisture content in corn ear," Sensors 16(12), 2196 (2016).
- <sup>3</sup>H. S. Roslan, M. A. M. Said, Z. Zakaria, M. H. Misran, N. Yusop, A. A. M. Bahar, and M. S. Y. Yusri, "High sensitivity microwave sensor for material characterization using square split ring resonator," in *Proceedings of IEEE International RF and Microwave Conference (RFM)* (IEEE, 2022), pp. 1–4.
- <sup>4</sup>X. Han, X. Li, Y. Zhou, Z. Ma, P. Peng, C. Fu, and L. Qiao, "Microwave sensor loaded with complementary curved ring resonator for material permittivity detection," IEEE Sens. J. **22**(21), 20456–20464 (2022).
- <sup>5</sup>A. A. Al-Behadili, I. A. Mocanu, N. Codreanu, and M. Pantazica, "Modified split ring resonators sensor for accurate complex permittivity measurements of solid dielectrics," Sensors 20(23), 6855 (2020).
- <sup>6</sup>P. K. Varshney and M. J. Akhtar, "Permittivity estimation of dielectric substrate materials via enhanced SIW sensor," IEEE Sens. J. **21**(10), 12104–12112 (2021).
- <sup>7</sup>N. S. Khair, N. A. T. Yusof, Y. A. Wahab, B. S. Bari, N. I. Ayob, and M. Zolkapli, "Substrate-integrated waveguide (SIW) microwave sensor theory and model in characterising dielectric material: A review," Sens. Int. 4, 100244 (2023).

- <sup>8</sup>Q. Chen, Z. Long, N. Shinohara, and C. Liu, "A substrate integrated waveguide resonator sensor for dual-band complex permittivity measurement," Processes 10(4), 708 (2022).
- <sup>9</sup>Y. Zhou, M. Mahmoud, and S. B. A. Rahim, "Design and optimization of interdigitated microwave sensor for multidimensional sensitive characterization of solid materials," Results Eng. 15, 100568 (2022).
- 10 M. Nosrati, F. Soltanian, and A. Nosrati, "Sensitivity enhancement of microwave split-ring-resonator sensors," IEEE Trans. Compon. Packag. Manuf. Technol. 14, 921 (2024).
- <sup>11</sup>C. Liu, S. Ghosh, and S. P. Kosta, "Computationally intelligent sensor system for microwave characterization of dielectric sheets," Heliyon 9(2), e13178 (2023).
   <sup>12</sup>M. A. Meor Said, M. K. A. Rahim, N. A. Samsuri, and A. A. A. Aziz.
- <sup>12</sup>M. A. Meor Said, M. K. A. Rahim, N. A. Samsuri, and A. A. A. Aziz, "Dielectric permittivity sensor based on planar open-loop resonator," Electronics 11(11), 1787 (2022).
- <sup>13</sup>O. Talmoudi, Á. G. Gómez, O. Fernández, T. F. Ibáñez, A. Tribak, and J. Terhzaz, "Design and analysis of a bandpass filter implemented in substrate integrated waveguide," Int. J. Microwave Opt. Technol. 19(4), 373 (2024).
- <sup>14</sup>A. Iqbal, J. J. Tiang, S. K. Wong, M. Alibakhshikenari, F. Falcone, and E. Limiti, "Miniaturization trends in substrate integrated waveguide (SIW) filters: A review," IEEE Access 8, 223287–223305 (2020).
- 15T. Haq, M. R. K. Krishna, and M. J. Akhtar, "Extremely sensitive microwave sensor for evaluation of dielectric characteristics of low-permittivity materials," Sensors 20(7), 1916 (2020).
- <sup>16</sup>M. A. H. Ansari, A. K. Jha, and M. J. Akhtar, "Design and application of the CSRR-based planar sensor for noninvasive measurement of complex permittivity," IEEE Sens. J. **15**(12), 7181–7189 (2015).
- <sup>17</sup>A. Ebrahimi, J. Scott, and K. Ghorbani, "Differential sensors using microstrip lines loaded with two split-ring resonators," IEEE Sens. J. 18(14), 5786–5793 (2018).
- 18 A. Kapoor, P. K. Varshney, and M. J. Akhtar, "Interdigital capacitor loaded electric-LC resonator for dielectric characterization," Microw. Opt. Technol. Lett. № 62(1), 2835 (2020).
- 19Z. Wei et al., "A high-sensitivity microfluidic sensor based on SIW re-entrant cavity," Sensors 18(11), 4005 (2018).